Dynamical properties of chemical systems near Hopf bifurcation points

Cite as: Chaos **10**, 791 (2000); https://doi.org/10.1063/1.1311980
Submitted: 30 December 1999 . Accepted: 19 July 2000 . Published Online: 30 November 2000

M. Ipsen and I. Schreiber

Dynamical properties of chemical systems near Hopf bifurcation points

M. Ipsen[a)]
Department of Physical Chemistry, Fritz-Haber-Institut der Max-Planck-Gesellschaft Faradayweg 4-6, D-14195 Berlin, Germany

I. Schreiber[b)]
Department of Chemical Engineering, Prague Institute of Chemical Technology, Technická 5, 166 28 Prague 6, Czech Republic

(Received 30 December 1999; accepted for publication 19 July 2000)

In this paper, we numerically investigate local properties of dynamical systems close to a Hopf bifurcation instability. We focus on chemical systems and present an approach based on the theory of normal forms for determining numerical estimates of the limit cycle that branches off at the Hopf bifurcation point. For several numerically ill-conditioned examples taken from chemical kinetics, we compare our results with those obtained by using traditional approaches where an approximation of the limit cycle is restricted to the center subspace spanned by critical eigenvectors, and show that inclusion of higher-order terms in the normal form expansion of the limit cycle provides a significant improvement of the limit cycle estimates. This result also provides an accurate initial estimate for subsequent numerical continuation of the limit cycle. © *2000 American Institute of Physics.* [S1054-1500(00)00404-3]

The oscillatory behavior of chemical systems near the onset of a Hopf bifurcation instability is of considerable importance since the discovery by Belousov of homogeneous oscillations in a cerium catalyzed oxidation of citric acid by bromate,[1] the following work of Zhabotinsky,[2] early observations of chemical waves,[3] and oscillations in a broad range of chemical systems.[4] Here the dynamics can be described efficiently by virtue of a center manifold theorem in a low-dimensional space by using so-called normal forms. In this paper, we show how the inclusion of higher-order terms from the normal form description leads to a significant improvement of the description of the chemical oscillatory kinetics near the Hopf bifurcation point. This approach gives a much more accurate description of the geometry of the limit cycle and, in addition, provides an accurate starting point suitable for further investigation of the dynamical properties of the limit cycle by numerical continuation.

I. INTRODUCTION

Oscillatory chemical reactions often exhibit a broad range of time scales. This is due to the fact that the rate constants governing the time scale of each elementary reaction may differ by several orders of magnitude. For this reason, analysis and simulation of chemical kinetics needs special care since the underlying ordinary differential equations (ODE's) typically are highly stiff and, therefore, numerically ill-conditioned. Examples of this dynamical behavior include the Belousov–Zhabotinsky reaction,[5] the horseradish peroxidase-oxidase reaction,[6,7] oscillatory behavior found in the metabolic decomposition of glucose,[8] and intracellular calcium oscillations.[9] In this paper, we focus attention on chemical systems where the oscillations originate from an instability of the Hopf bifurcation type and discuss the numerical problems encountered when locating and analyzing properties of oscillatory behavior close to the Hopf bifurcation point.

Assume that two complex eigenvalues associated with the linearization of the flow around a stationary solution become purely imaginary when certain model parameters are varied. Then the dynamical system undergoes a Hopf bifurcation[10–13] causing a small-amplitude limit cycle to branch off at the Hopf bifurcation point. The limit cycle close to the bifurcation point lies in a two-dimensional unfolding of the center manifold tangent to a linear subspace spanned by the real and imaginary parts of the complex eigenvector associated with the bifurcating complex eigenvalue.[14]

As a consequence of the center manifold theorem,[14–16] the behavior of the original system can be represented by a much simpler two-dimensional ordinary differential equation called a normal form which, sufficiently close to the bifurcation point, describes the oscillations on a quantitative level. From this point of view, the normal form becomes a universal dynamical system whose characteristics are valid for any dynamical system which undergoes a Hopf bifurcation.

In a vast majority of systems, the presence of the Hopf bifurcation is a necessary prerequisite for the onset of more complex dynamical phenomena in the system. Indeed, dynamic events such as quasi-periodic oscillations, sequences of period doublings, and chaos can very often be traced back as originating from a Hopf bifurcation. Limit cycles, however, may arise in other ways as well, for example, via a saddle node or a homoclinic bifurcation.

In model studies of such phenomena, one typically applies continuation techniques to observe how dynamical characteristics of limit sets vary as a function of some relevant parameter (for further details regarding the theory and

a)Electronic mail: Ipsen@fhi-berlin.mpg.de
b)Electronic mail: Igor.Schreiber@vscht.cz

numerical aspects of continuation, we refer to the detailed reviews presented in Refs. 16 and 17). For continuation of limit cycles, the Hopf bifurcation provides a natural starting point, since the normal form equation may be used to generate precise initial estimates of the limit cycle originating at the bifurcation point. This estimate may then serve as initial input data for the actual continuation algorithm used. Numerical codes for solving this particular task, such as BIFOR2,[12] have been available for many years. Even though we focus on examples taken from nonlinear chemical kinetics, we emphasize that the results presented are generally applicable for any dynamical system represented by a set of autonomous ordinary differential equations.

In Sec. II, we briefly review how the center manifold can be used to derive higher-order terms of the expansion of the limit cycle that branches off at the Hopf bifurcation point. Section III briefly outlines how to numerically find a Hopf bifurcation point and calculate quantities needed to evaluate the bifurcation formulas.

In Sec. IV, we demonstrate by several examples, that the higher-order terms provide a significant improvement in the accuracy of the calculated limit cycle compared to other approaches even quite far from the bifurcation point. This in turn enables one to safely start numerical continuation even in cases when highly unstable modes occur due to the presence of unstable eigendirections.

The Hopf and other bifurcation curves for these examples were calculated by the continuation package CONT [Ref. 18 (Appendix B)].

II. REVIEW OF THEORY

The normal form approach utilizes the fact that the center manifold can be parameterized by a linear tangent space called the center subspace which is spanned by the eigenvectors associated with the bifurcating eigenvalues. In particular, we may choose these eigenvectors as a basis for the center subspace implying that the parametrization can be expressed in terms of an expansion in coordinates of the eigenspace. These coordinates are called amplitudes. The dynamical evolution of the system can then be expressed by the time dependence of these amplitudes determined by a differential equation referred to as a normal form or amplitude equation. In this section, we present a summary of the derivation of the amplitude equation for the Hopf bifurcation.

We start by considering a set of autonomous ordinary differential equations described by

$$\dot{\mathbf{x}}=\mathbf{F}(\mathbf{x},\mu)=\mathbf{J}\cdot\mathbf{x}+\mathbf{f}(\mathbf{x},\mu), \tag{1}$$

where the right-hand-side explicitly has been split into linear and nonlinear parts $\mathbf{J}\cdot\mathbf{x}$ and $\mathbf{f}(\mathbf{x},\mu)$ respectively. In Eq. (1), the vector $\mathbf{x}\in\mathbb{R}^n$ describes a set of n (chemical or physical) quantities, whose derivative with respect to time is described by the vector field $\mathbf{F}:\mathbb{R}^n\mapsto\mathbb{R}^n$. The variable $\mu\in\mathbb{R}$ denotes a scalar quantity, which here will serve as a bifurcation parameter.

We now consider stationary solutions $\mathbf{x}_s$ of Eq. (1). Assume that a parameter value of μ exists such that the linearization $\mathbf{J}$ of the right-hand-side of Eq. (1) has two complex conjugate, pure imaginary eigenvalues $\lambda=i\omega_0$ and $\bar{\lambda}=-i\omega_0$ (all other eigenvalues are assumed to have nonzero real parts). In the following, we shall for simplicity assume that this situation occurs for $\mathbf{x}_s=\mathbf{0}$ and $\mu=0$ (this situation can always be achieved by a simple linear translation of the stationary point and the parameter value). We denote the right and left eigenvectors of $\mathbf{J}$ corresponding to λ by $\mathbf{u}$ and $\mathbf{u}^*$, and those of $\bar{\lambda}$ by $\bar{\mathbf{u}}$ and $\bar{\mathbf{u}}^*$, and choose these eigenvectors normalized according to

$$\mathbf{u}\cdot\mathbf{u}^*=1,\quad \mathbf{u}\cdot\bar{\mathbf{u}}^*=0,\quad \bar{\mathbf{u}}\cdot\mathbf{u}^*=0,\quad \bar{\mathbf{u}}\cdot\bar{\mathbf{u}}^*=1. \tag{2}$$

As a consequence of the center manifold theorem,[14,15] the branching which takes place at a Hopf bifurcation point, is restricted to a two-dimensional center manifold W^c tangent to the linear center subspace E^c spanned by the real and imaginary parts of the right eigenvector $\mathbf{u}$. To describe the branching we may, therefore, restrict ourselves to studying the dynamics of the system (1) on the center manifold. This can be achieved in the following way:

For points $\mathbf{x}\in W^c$, we may construct a transformation $\mathbf{x}=\mathbf{z}+\mathbf{h}(\mathbf{z},\mu)$, which maps points $(\mathbf{z},\mu)$ from $E^c\times\mathbb{R}$ to points $\mathbf{z}+\mathbf{h}(\mathbf{z},\mu)$ on the center manifold. If we write the vector $\mathbf{z}$ as $\mathbf{z}=z\mathbf{u}+\bar{z}\bar{\mathbf{u}}$, we obtain a complex differential equation for the motion in $E^c\times\mathbb{R}$ of the form

$$\dot{z}=i\omega_0 z+\mathbf{u}^*\cdot\mathbf{g}(\mathbf{z},\mu). \tag{3}$$

The functions $\mathbf{F}(\mathbf{z}+\mathbf{h}(\mathbf{z},\mu),\mu)$, $\mathbf{h}(\mathbf{z},\mu)$, and $\mathbf{g}(\mathbf{z},\mu)$ are now Taylor expanded as

$$\begin{aligned}\mathbf{h}(\mathbf{z},\mu)&=\sum_{pqr}\mathbf{h}_{pqr}z^p\bar{z}^q\mu^r,\quad \mathbf{g}(\mathbf{z},\mu)=\sum_{pqr}\mathbf{g}_{pqr}z^p\bar{z}^q\mu^r,\\ \mathbf{F}(\mathbf{z}+\mathbf{h}(\mathbf{z},\mu),\mu)&=\mathbf{J}\cdot\mathbf{z}+\sum_{pqr}\mathbf{f}_{pqr}z^p\bar{z}^q\mu^r.\end{aligned} \tag{4}$$

The coefficients $\mathbf{g}_{pqr}$ and $\mathbf{h}_{pqr}$ can then be obtained order by order by the following iterative procedure. At any order (p,q,r), any nonvanishing component $\mathbf{u}^*\cdot\mathbf{g}_{pqr}$ in the amplitude equation is given explicitly by

$$\mathbf{u}^*\cdot\mathbf{g}_{pqr}=\mathbf{u}^*\cdot\mathbf{f}_{pqr}, \tag{5}$$

which only appears if the resonance condition,

$$p-q=1, \tag{6}$$

is satisfied for the terms indicated at order (p,q,r). The amplitude equation includes all resonant terms and no others. To obtain the coefficient $\mathbf{h}_{pqr}$, one has to solve the system of linear equations

$$(\mathbf{J}-(p-q)\lambda\mathbf{I})\cdot h_{pqr}=-\mathbf{Q}\cdot\mathbf{\Phi}_{pqr}, \tag{7}$$

determining the nonresonant components of $\mathbf{h}_{pqr}$. Here $\mathbf{Q}$ is the projection onto the nonresonant part of E^c defined by $\mathbf{Q}\cdot\mathbf{x}=\mathbf{x}-(\mathbf{u}^*\cdot\mathbf{x})\mathbf{u}$. The auxiliary condition,

$$\mathbf{u}^*\cdot\mathbf{h}_{pqr}=\mathbf{0}, \tag{8}$$

ensures that all resonant components of $\mathbf{h}_{pqr}$ vanish. Equation (7) together with Eq. (8) determines $\mathbf{h}_{pqr}$ completely.

To cubic order, the amplitude transformation for the Hopf bifurcation is

TABLE I. Formulas for calculating the coefficients of the normal form transformation and the normal form for the Hopf bifurcation. At the bifurcation, the Jacobian $\mathbf{J}$ has two complex conjugate eigenvectors $\mathbf{u}$ and $\overline{\mathbf{u}}$ and left eigenvectors $\mathbf{u}^*$ and $\overline{\mathbf{u}}^*$ corresponding to critical eigenvalues $\lambda = i\omega_0$ and $\overline{\lambda} = -i\omega_0$. The normal form transformation $\mathbf{x} = \mathbf{z} + \mathbf{h}(\mathbf{z},\mu)$, $\mathbf{z} = \mathbf{u}z + \overline{\mathbf{u}z}$, transforms a solution $z(t)$ of the normal form to the motion $\mathbf{x}(t)$ on the unfolded center manifold for the dynamical system. The vector coefficients $\mathbf{h}_{pqr}$ are determined as solutions to the linear equations indicated, in terms of the derivatives of the vector field $\mathbf{F}$. The coefficients of the normal form can then be found through the explicit expressions indicated, in terms of $\mathbf{F}$ and $\mathbf{h}_{pqr}$.

Formulas for Hopf Bifurcation		
Transformation $\mathbf{x} = \mathbf{z} + \mathbf{h}(\mathbf{z},\mu)$		$\mathbf{x} = \mathbf{u}z + \overline{\mathbf{u}z} + \mathbf{h}_{200}z^2 + \mathbf{h}_{110}\lvert z\rvert^2 + \mathbf{h}_{020}\overline{z}^2 + \mathbf{h}_{300}z^3 + \mathbf{h}_{210}\lvert z\rvert^2 z + \mathbf{h}_{120}\lvert z\rvert^2\overline{z} + \mathbf{h}_{030}\overline{z}^3 + \mathbf{h}_{001}\mu + (\mathbf{h}_{101}z + \mathbf{h}_{011}\overline{z})\mu$
Linear equations for h_{pqr}		$(\mathbf{J} - 2i\omega_0\mathbf{I})\cdot\mathbf{h}_{200} = -\frac{1}{2}\mathbf{F}_{\mathbf{xx}}(\mathbf{u},\mathbf{u})$
	z^2:	$\mathbf{h}_{020} = \overline{\mathbf{h}}_{200}$
	$\lvert z\rvert^2$:	$\mathbf{J}\cdot\mathbf{h}_{110} = -\mathbf{F}_{\mathbf{xx}}(\mathbf{u},\overline{\mathbf{u}})$
		$(\mathbf{J} - 3i\omega_0\mathbf{I})\cdot\mathbf{h}_{300} = -\frac{1}{2}\mathbf{F}_{\mathbf{xx}}(\mathbf{u},\mathbf{h}_{200}) - \frac{1}{6}\mathbf{F}_{\mathbf{xxx}}(\mathbf{u},\mathbf{u},\mathbf{u})$,
	z^3:	$\mathbf{h}_{03} = \overline{\mathbf{h}}_{300}$
	$z\lvert z\rvert^2$:	$(\mathbf{J} - i\omega_0\mathbf{I})\cdot\mathbf{h}_{210} = -\mathbf{Q}\cdot(\mathbf{F}_{\mathbf{xx}}(u,\mathbf{h}_{110}) + \mathbf{F}_{\mathbf{xx}}(\overline{\mathbf{u}},\mathbf{h}_{200}) + \frac{1}{2}\mathbf{F}_{\mathbf{xxx}}(\mathbf{u},\mathbf{u},\overline{\mathbf{u}}))$
		$\mathbf{u}^*\cdot\mathbf{h}_{210} = 0$
	μ:	$\mathbf{J}\cdot\mathbf{h}_{001} = \overline{\mathbf{h}}_{2\mathbf{F}_\mu}$
		$(\mathbf{J} - i\omega_0\mathbf{I})\cdot\mathbf{h}_{101} = -\mathbf{Q}\cdot(\mathbf{F}_{\mathbf{x}\mu}\mathbf{u} + \mathbf{F}_{\mathbf{xx}}(\mathbf{u},\mathbf{h}_{001}))$
		$\mathbf{u}^*\cdot\mathbf{h}_{101} = 0$
	μz:	$\mathbf{h}_{011} = \overline{\mathbf{h}}_{101}$
		$\mathbf{Q}\cdot\mathbf{x} = \mathbf{x} - (\mathbf{u}^*\cdot\mathbf{x})\mathbf{u}$
Resonant coefficients		$g = \mathbf{u}^*\cdot\mathbf{F}_{\mathbf{xx}}(\mathbf{u},\mathbf{h}_{110}) + \mathbf{u}^*\cdot\mathbf{F}_{\mathbf{xx}}(\overline{\mathbf{u}},\mathbf{h}_{200}) + \frac{1}{2}\mathbf{u}^*\cdot\mathbf{F}_{\mathbf{xxx}}(\mathbf{u},\mathbf{u},\overline{\mathbf{u}})$
		$\lambda_1 = \mathbf{u}^*\cdot\mathbf{F}_{x\mu}\cdot\mathbf{u} + \mathbf{u}^*\cdot\mathbf{F}_{\mathbf{xx}}(\mathbf{u},\mathbf{h}_{001})$
Amplitude equation		$\dot{z} = (i\omega_0 + \lambda_1\mu)z + gz\lvert z\rvert^2$

$$\mathbf{x} = \mathbf{u}z + \overline{\mathbf{u}z} + \mathbf{h}_{200}z^2 + \mathbf{h}_{110}|z|^2 + \mathbf{h}_{020}\overline{z}^2 + \mathbf{h}_{300}z^3 + \mathbf{h}_{210}|z|^2 z + \mathbf{h}_{120}|z|^2\overline{z} + \mathbf{h}_{030}\overline{z}^3 + \mathbf{h}_{001}\mu + (\mathbf{h}_{101}z + \mathbf{h}_{011}\overline{z})\mu, \tag{9}$$

with the corresponding amplitude equation

$$\dot{z} = (i\omega_0 + \lambda_1\mu)z + gz|z|^2, \tag{10}$$

where λ_1 and g are given by

$$\lambda_1 = \mathbf{u}^*\cdot\mathbf{F}_{\mathbf{x}\mu}\cdot\mathbf{u} + \mathbf{u}^*\cdot\mathbf{F}_{\mathbf{xx}}(\mathbf{u},\mathbf{h}_{001}), \tag{11a}$$

$$g = \mathbf{u}^*\cdot\mathbf{F}_{\mathbf{xx}}(\mathbf{u},\mathbf{h}_{110}) + \mathbf{u}^*\cdot\mathbf{F}_{\mathbf{xx}}(\overline{\mathbf{u}},\mathbf{h}_{200}) + \tfrac{1}{2}\mathbf{u}^*\cdot\mathbf{F}_{\mathbf{xxx}}(\mathbf{u},\mathbf{u},\overline{\mathbf{u}}). \tag{11b}$$

The derivation of the explicit expressions that define these coefficients is standard and is summarized in a compact form in Table I. For details regarding the derivation, see the discussions in Refs. 16 and 19.

In particular, if we represent the complex variable z in polar form $z = R\exp(\mathrm{i}\theta)$ and require the amplitude R to be stationary in time, we find the following simple solution to the normal form (10)

$$R_s = \sqrt{-\sigma_1\mu/g^r}, \quad \theta(t) = \omega_0 t + \left(\omega_1 - \sigma_1\frac{g^i}{g^r}\right)\mu t, \tag{12}$$

corresponding to a solution with a constant amplitude and phase varying linearly in time. Observe that we have introduced the notation $g = g^r + \mathrm{i}g^i$ and $\lambda_1 = \sigma_1 + \mathrm{i}\omega_1$ in Eq. (12). Inserting this solution into the corresponding transformation $\mathbf{h}(\mathbf{z},\mu)$ given by Eq. (9) yields the following expansion which corresponds to a (periodic) limit cycle solution for the differential equation (1) on the center manifold associated with the Hopf bifurcation

$$\mathbf{x} = \mathbf{x}_s + \mathbf{h}_{001}\mu + \mathbf{x}_1(t) + \mathbf{x}_2(t) + \mathbf{x}_3(t), \tag{13}$$

where

$$\mathbf{x}_1(t) = R_s(\mathbf{u}e^{\mathrm{i}\theta} + \text{c.c.}), \tag{14}$$

$$\mathbf{x}_2(t) = R_s^2(\mathbf{h}_{200}e^{2i\theta} + \text{c.c.} + \mathbf{h}_{110}), \tag{15}$$

$$\mathbf{x}_3(t) = R_s^3(\mathbf{h}_{300}e^{3i\theta} + \mathbf{h}_{210}e^{\mathrm{i}\theta} + \text{c.c.}) + R_s(\mathbf{h}_{101}e^{\mathrm{i}\theta} + \text{c.c.})\mu, \tag{16}$$

where c.c. denotes the complex conjugate of the preceding terms within a given bracket.

The stability of the limit cycle is determined by the real part g^r of the nonlinear coefficient g in Eq. (10). If $g^r < 0$ the limit cycle is stable (within the center manifold) and it is unstable for $g^r > 0$. In each of the two cases, the Hopf bifurcation is referred to as being either supercritical or subcritical respectively. For a given distance μ from the bifurcation point, the period T of the limit cycle can be determined from Eq. (12) as

$$T(\mu) = \frac{2\pi}{\omega_0 + (\omega_1 - \sigma_1 g^i/g^r)\mu}. \tag{17}$$

The third-order expansion (13) of the limit cycle illustrates the well-known fact that the limit cycle which bifurcates from the Hopf bifurcation is analytic in the square root of the distance $|\mu|$ from the bifurcation point. The term $\mathbf{h}_{001}$ is not directly related to the geometry of the limit cycle itself but corresponds to the first-order derivative of the stationary point $\mathbf{x}_s$ with respect to μ. This term therefore provides a first-order description of the translation of the stationary point as the distance from the bifurcation point μ is varied. The time dependent term $\mathbf{x}_1(t)$ corresponds to the linear description of the limit cycle which is obtained by projecting Eq. (13) onto the center subspace E^c. By means of perturbation theory,[20] one can show that the part of $\mathbf{x}_3(t)$ which involves $\mathbf{h}_{101}$ can be identified as describing the rotation of the eigenvector $\mathbf{u}$ per unit change of μ. Similarly, we may identify the coefficient λ_1 in the normal form Eq. (10) as the derivative of the bifurcating eigenvalue with respect to μ.

By inspection of Table I, we also observe that explicit calculations of the coefficient vectors $\mathbf{h}_{001}$, $\mathbf{h}_{200}$, and $\mathbf{h}_{110}$ are needed in order to determine the complex resonant coefficients λ_1 and g in Eq. (10). For this reason, the terms $\mathbf{x}_1(t)$ and $\mathbf{x}_2(t)$ in the expansion (13) of the limit cycle are immediately available once the resonant coefficients in the normal form have been determined. However, to find the coefficient vectors $\mathbf{h}_{300}$, $\mathbf{h}_{210}$, and $\mathbf{h}_{101}$ that determine the third-order term $\mathbf{x}_3(t)$, observe that an additional set of linear equations must be solved.

One crude approach for estimating the limit cycle emanating from a Hopf bifurcation is to use only a simplification of the term $\mathbf{x}_1(t)$ in order to estimate a point $\mathbf{x}$ on the limit cycle with corresponding period T, namely

$$\mathbf{x}=\epsilon(\mathbf{u}+\overline{\mathbf{u}}),$$

$$T=\frac{2\pi}{\omega_0}, \tag{18}$$

for some real (small) value of ϵ. This expansion is then applied for fixed $\mu=\epsilon$, which will hold sufficiently close to the bifurcation point since the derivative $dR_s/d\mu$ is infinite at $\mu=0$. However, for systems where the limit cycle is unstable due to either a subcritical Hopf bifurcation or a stationary point associated with some very unstable nonbifurcating eigendirections, the estimate provided by Eq. (18) will rarely suffice as initial input data for a continuation algorithm. This in particular applies to methods using a shooting method in solving the associated boundary value problem. Here either one or (if multiple shooting is required) several precise estimates of points on the limit cycle are needed as initial input data for the continuation problem. In Sec. IV, we shall address this problem by discussing several examples which illustrate the importance and advantages obtained when the full expansion (13) is used instead of the traditional approach represented by Eq. (18). Also, the Hopf bifurcation frequently turns out to be subcritical, and the bifurcating unstable cycle typically merges with a stable cycle in a fold bifurcation at a nearby parameter value. A normal form capturing this feature requires the inclusion of terms of quintic order in the expansion. Even though this extension is straightforward, we do not discuss it here, but rather use continuation to determine the location of the fold bifurcation.

First however, we describe shortly the numerical algorithm used in the results presented here for locating Hopf bifurcation solutions $(\mathbf{x}, \mu)$ to Eq. (1).

III. LOCATION OF HOPF BIFURCATION POINTS AND CALCULATION OF NORMAL FORM COEFFICIENTS

Several approaches for location of Hopf bifurcation points exist as described in the reviews given in Refs. 12, 16, 17, and 21. In the work presented in this paper, we have chosen a slightly modified variant of the algorithm described in Ref. 22. Here the equations that define the Hopf bifurcation point are

$$\mathbf{F}(\mathbf{x}_s,\mu)=\mathbf{0}, \tag{19a}$$

$$\mathbf{J}\cdot\mathbf{v}_1+\omega_0\mathbf{v}_2=\mathbf{0}, \tag{19b}$$

$$\mathbf{J}\cdot\mathbf{v}_2-\omega_0\mathbf{v}_1=\mathbf{0}, \tag{19c}$$

$$\mathbf{v}_1^T\cdot\mathbf{v}_1+\mathbf{v}_2^T\cdot\mathbf{v}_2=1, \tag{19d}$$

$$\mathbf{v}_2^T\cdot\mathbf{v}_1=0, \tag{19e}$$

where Eq. (19) constitutes a system of $3n+2$ nonlinear equations in $3n+2$ unknowns: the stationary point $\mathbf{x}_s$, the bifurcation parameter μ, the imaginary part ω_0 of the bifurcating eigenvalue, and the real and imaginary parts $\mathbf{v}_1$ and $\mathbf{v}_2$ of the complex eigenvector $\mathbf{u}$ associated with the bifurcating eigenvalue. The solution of this system is readily obtained by applying a standard Newton iteration scheme to Eq. (19).

Even though the set of defining equations has a large dimension compared to other approaches which typically involve numerical evaluation of determinants, we find it numerically more stable than low-dimensional schemes since determinant evaluations easily become numerically very ill-behaved. Furthermore, in situations where the purpose of solving Eq. (19) is to provide an initial estimate of the limit cycle solution of Eq. (1), one typically analyzes only a few Hopf bifurcation points. Even for larger system sizes (we have made tests for $n=256$) such computations proceed smoothly on modern workstations or high-end PC's.

Notice that setting up a Newton algorithm for the system (19) requires the evaluation of second-order derivatives of Eq. (1) with respect to $\mathbf{x}$ and μ—the so-called Hessian. This can either be supplied in symbolic form or be obtained by numerical differentiation. In the implementation presented in this paper, we have used a symmetric five-point differentiation formula Ref. 23 (p. 914) to evaluate the Hessian using analytic expressions for the elements of the Jacobian. The structure of the Jacobian matrix associated with Eq. (19) and explicit expressions for all its elements are shown in Fig. 1 and Table II, respectively. The matrix is relatively sparse and the linear equations arising from Newton iteration of Eq. (19) can be solved efficiently using a block decomposition described in Ref. 24.

Once the Newton iteration has converged, the formulas in Table I must be evaluated in order to find the terms in the expansion (13) as well as other properties of the limit cycle. Solutions of the linear equations that determine the vectors

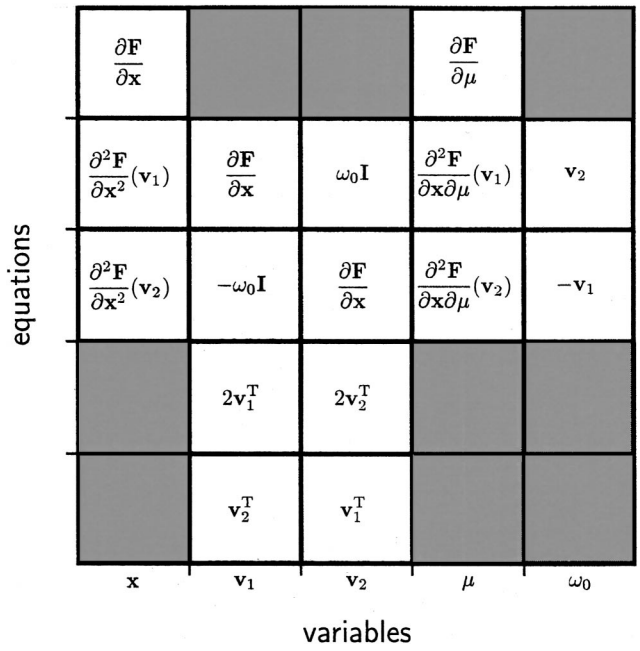

FIG. 1. Structure of the Jacobian matrix needed to solve the defining system (19) for locating a Hopf bifurcation point by Newton iteration. Gray colored areas contain zero elements only. Explicit expressions needed to evaluate each nonzero matrix element are shown in Table II.

$\mathbf{h}_{200}$, $\mathbf{h}_{110}$, and $\mathbf{h}_{001}$ is a straightforward task using standard linear algebra routines from numerical libraries such as LAPACK.[25] After this step has been accomplished, the resonant coefficients λ_1 and g may be determined by projecting the vectors $\mathbf{\Phi}_{210}$ and $\mathbf{\Phi}_{101}$ onto the center subspace. Notice that the calculation of g in general requires evaluation of the third-order derivatives of Eq. (1). In the examples considered here, these were calculated numerically from the Jacobian of Eq. (1) using a symmetric four point formula Ref. 23 (p. 884).

The vectors $\mathbf{h}_{300}$, $\mathbf{h}_{210}$, and $\mathbf{h}_{101}$ should now be found. Since the linear equation which determines $\mathbf{h}_{300}$ is regular, this vector is readily obtained. However, the linear systems that define $\mathbf{h}_{210}$ and $\mathbf{h}_{101}$ involve the singular matrix $\mathbf{J}-i\omega_0\mathbf{I}$. First the singular part of the vector $\mathbf{\Phi}_{210}$ and $\mathbf{\Phi}_{101}$ are removed according to Eq. (7). The resulting system is then solved using a singular value decomposition where the solution is subject to the additional condition (8).

Next assume that we would like to know the parameter dependence of the limit cycle throughout a broad region by means of a numerical continuation procedure. The formulas in Table I provides us readily with an initial estimate for such a calculation. To choose a proper operating point for the initial estimate of the limit cycle, a finite parameter distance from the bifurcation point must be chosen. This value is finally used in Eq. (13) to generate either one or, if a multiple shooting or a discretization is desired, a set of initial points on the limit cycle. An estimate for the initial period of the limit cycle is given by Eq. (17).

TABLE II. Expressions for the elements of the Jacobian matrix shown in Fig. 1 needed to solve the defining system (19) for locating a Hopf bifurcation point by Newton iteration.

Block	Size	Element expression
$\left(\frac{\partial \mathbf{F}}{\partial \mathbf{x}}\right)_{ij}$	$(n\times n)$	$\frac{\partial F_i}{\partial x_j}$
$\left(\frac{\partial \mathbf{F}}{\partial \mu}\right)_{i}$	$(n\times 1)$	$\frac{\partial F_i}{\partial \mu}$
$\left(\frac{\partial^2 \mathbf{F}}{\partial \mathbf{x}^2}(\mathbf{v}_1)\right)_{ij}$	$(n\times n)$	$\sum_{k=1}^{n}\frac{\partial^2 F_i}{\partial x_j \partial x_k} v_{1k}$
$\left(\frac{\partial^2 \mathbf{F}}{\partial \mathbf{x}^2}(\mathbf{v}_2)\right)_{ij}$	$(n\times n)$	$\sum_{k=1}^{n}\frac{\partial^2 F_i}{\partial x_j \partial x_k} v_{2k}$
$\left(\frac{\partial^2 \mathbf{F}}{\partial \mathbf{x}\partial \mu}(\mathbf{v}_1)\right)_{i}$	$(n\times 1)$	$\sum_{k=1}^{n}\frac{\partial^2 F_i}{\partial x_k \partial \mu} v_{1k}$
$\left(\frac{\partial^2 \mathbf{F}}{\partial \mathbf{x}\partial \mu}(\mathbf{v}_2)\right)_{i}$	$(n\times 1)$	$\sum_{k=1}^{n}\frac{\partial^2 F_i}{\partial x_k \partial \mu} v_{2k}$

IV. EXAMPLES

In this section, we examine four different models in order to discuss and illustrate the use of Eq. (13) to approximate the geometry of limit cycles emerging from a Hopf bifurcation. The examples are arranged according to the size of their phase space. While the dynamics of the first and the fourth models are amenable to numerical integration by standard Runge–Kutta solvers, the other two models are highly stiff and a relevant numerical solver has to be used (e.g., LSODE[26]). In order to compare the expansion in Eq. (13) with the exact limit cycle solutions, we have introduced the following root-mean-square measure:

$$|\mathbf{x}| = \sqrt{\frac{1}{T}\int_0^T \sum_{j=1}^{n} x_j(t)^2 dt}. \tag{20}$$

The relative error $|\mathbf{x}_i|_{\mathrm{rel}}$, for a given expansion $\mathbf{x}_i(t)$ of Eq. (13) of order $i=1,...,3$, is then calculated as $|\mathbf{x}_i|_{\mathrm{rel}}=|\mathbf{x}-\mathbf{x}_i|/|\mathbf{x}|$ where $\mathbf{x}(t)$ is the exact limit cycle solution determined by numerical continuation.

A. Papain oscillator

The first model example is the papain oscillator—a biochemical model involving the enzyme papain. This system describes the enzyme catalyzed hydrolysis of a substrate (N-α-benzoyl-L-arginin ethylester) in a compartment connected to a reservoir.[27,28] The model can be cast in terms of two independent variables s (dimensionless substrate concentration) and h (dimensionless concentration of hydrogen ions) whose temporal dynamics are described by the following differential equations:

$$\begin{aligned} \dot{s} &= q_S(s_0 - s) - r_{HS}, \\ \dot{h} &= \frac{h^2}{1+h^2}\left(q_H(h_0 - h) - \left(\frac{1}{h_0} - \frac{1}{h}\right) + r_{HS}\right), \end{aligned} \tag{21}$$

where the reaction kinetics term is

$$r_{HS} = Da\,\frac{s}{(f_1+f_2)s+f_3}, \tag{22a}$$

$$f_1 = (1 + 10^{-2.71}h + 10^{-1.49}h^{-1}), \tag{22b}$$

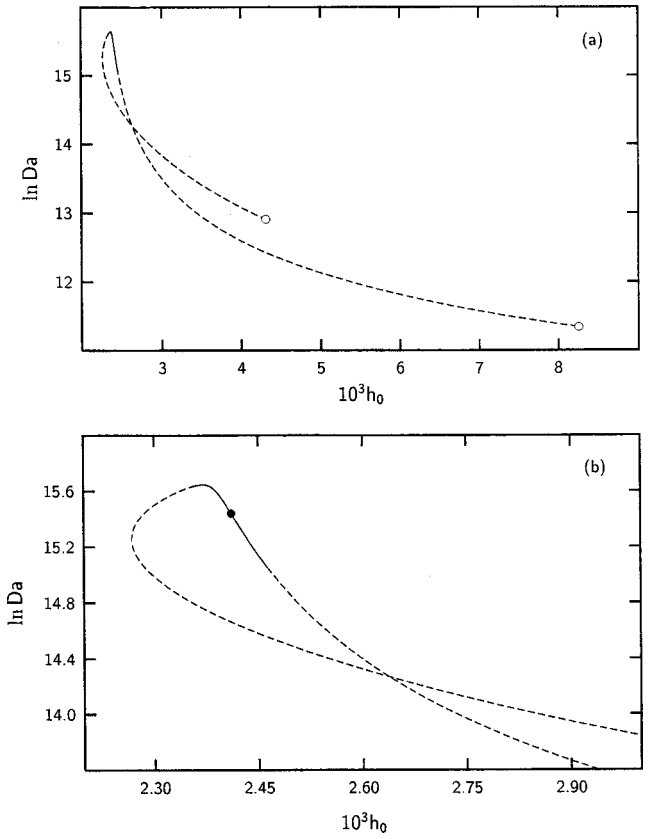

FIG. 2. Bifurcation diagram showing the locations of Hopf bifurcations for the papain oscillator defined in Eq. (21) in the plane of the two parameters h_0 and Da.

$$f_2 = 3.212(1 + 10^{-3.08} h), \tag{22c}$$

$$f_3 = 5.45 \times 10^{-5} f_1, \tag{22d}$$

and the values of fixed parameters are $q_S = 0.375, q_H = 1.766, s_0 = 1150$. The two remaining parameters, the Damköhler number Da, and the inflow concentration of hydrogen ions h_0 are used as bifurcation parameters.

The papain oscillator Eq. (21) exhibits a curve of Hopf bifurcations in the $h_0 - Da$ parameter space shown in the bifurcation diagram in Fig. 2(a). Both super- and subcritical bifurcations occur as shown in the figure with solid and dashed lines respectively. Both endpoints of the bifurcation curve terminate at codimension-two Bogdanov–Takens bifurcation points[29] where the Hopf bifurcation curve coalesces with a fold (or saddle-node) bifurcation curve (indicated with white circles). A blow-up of the region corresponding to supercritical bifurcations is shown in Fig. 2(b).

To investigate the effect of the nonlinear terms of the expansion (13), we have chosen the sample point $(h_0, \ln Da) = (2.410\,914 \times 10^{-3}, 15.439\,57)$ within the supercritical region as indicated on Fig. 2 with a solid circle, see also Table III. To study the limit cycle bifurcating from this point, we need to operate at a finite distance from the bifurcating point which is done by fixing Da and choosing $h_0 = 2.410\,778 \times 10^{-3}$. The comparison of the numerically accurate limit cycle solution obtained by the shooting method[17] and the estimates provided by Eq. (13) are shown as both time plots and phase portraits in Fig. 3. The first-order expansion of Eq. (13) shows large deviations from the exact solution, whereas the second- and third-order expansions agree increasingly better with the accurate solution. This is in correspondence with the relative deviations from the exact limit cycle solution given by Eq. (20), where we find 0.2254%, 0.0234%, and 0.0171% for the first-, second-, and third-order expansions respectively.

TABLE III. Characteristic coefficients for the normal form (10) associated with the Hopf bifurcation point in the papain model (21) indicated on the bifurcation diagram in Fig. 2 with a solid circle.

	Re	Im
h_0	$2.410\,914 \times 10^{-3}$	
D_a	$1.543\,957 \times 10^{1}$	
ω_0	2.537 017	
λ_1	$-1.778\,058 \times 10^{5}$	$6.838\,568 \times 10^{4}$
g	$1.955\,117 \times 10^{-1}$	$7.351\,983 \times 10^{-2}$

Numerical values for all the coefficient vectors used in the expansion Eq. (13) are shown in Table IV.

B. Inorganic pH oscillator

The next model by Luo and Epstein[30] has been used as a general system to describe pH oscillations in inorganic chemical reaction systems. This four variable model describes a flow-through stirred chemical system with inflow of

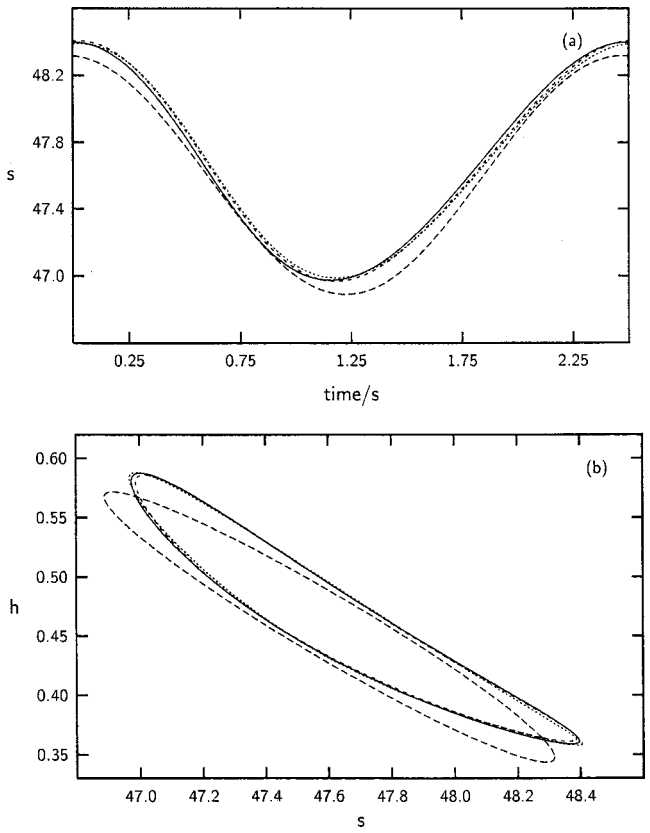

FIG. 3. Comparisons of the actual periodic solution (solid line) to the papain model (21) and its approximation by the first-, second-, and third-order expansions of the limit cycle formula (13) (long-dashed, short-dashed, and dotted lines, respectively).

TABLE IV. Numerical values for all characteristic vectors describing the Hopf bifurcation in the papain model (21) indicated on Fig. 2 with a solid circle. The coefficient vectors $\mathbf{h}_{ijk}$ have been calculated using the formulas of Table I. Observe that these are dependent on the chosen normalization of the complex right eigenvector $\mathbf{u}$. All shown numbers are needed to evaluate the terms in Eq. (13) describing the expansion of the limit cycle associated with the Hopf bifurcation point.

		Eigenvalues	
Stationary point $\mathbf{x}_s$	Vector field $\mathbf{F}(\mathbf{x}_s)$	Re	Im
$4.760\,271\times10^{1}$	$8.729\,991\times10^{-15}$	$8.881\,547\times10^{-15}$	2.537 017
$4.576\,065\times10^{-1}$	$-1.644\,461\times10^{-15}$	$8.881\,547\times10^{-15}$	−2.537 017

	Re	Im		Re	Im
$\mathbf{u}$	1.000 000	0.0	h_{200}	$2.117\,957\times10^{-2}$	$-1.639\,703\times10^{-1}$
	$-1.538\,992\times10^{-1}$	$-4.311\,294\times10^{-2}$		$3.103\,329\times10^{-2}$	$5.179\,438\times10^{-2}$
$\mathbf{u}^*$	$5.000\,000\times10^{-1}$	1.784 837	h_{210}	$-2.820\,617\times10^{-1}$	$1.626\,107\times10^{-1}$
	0.0	$1.159\,745\times10^{1}$		$3.639\,843\times10^{-2}$	$-3.718\,616\times10^{-2}$
$\mathbf{h}_{110}$	$3.184\,915\times10^{-1}$	$-2.139\,060\times10^{-10}$	h_{300}	$-4.455\,946\times10^{-2}$	$1.038\,566\times10^{-2}$
	$6.324\,371\times10^{-2}$	$3.282\,530\times10^{-11}$		$9.965\,680\times10^{-3}$	$-2.280\,003\times10^{-2}$
$\mathbf{h}_{001}$	0.0		h_{101}	$-1.031\,348\times10^{5}$	$2.952\,168\times10^{5}$
	$-2.723\,473\times10^{5}$			$3.144\,690\times10^{3}$	$-4.988\,006\times10^{4}$

reactants and outflow of reaction products whose dynamics are described by the following coupled set of ordinary differential equations:

$$\begin{aligned}
\dot{H} &= k_{-1}Z - k_1XH - k_2AHZ + 3k_3YZ - k_5BH \\
&\quad + k_0(H_0 - H), \\
\dot{X} &= k_{-1}Z - k_1XH + k_0(X_0 - X), \\
\dot{Y} &= k_2AHZ - k_3YZ - k_4Y - k_0Y, \\
\dot{Z} &= k_1XH - k_{-1}Z - k_2AHZ - k_3YZ - k_0Z.
\end{aligned} \tag{23}$$

Despite its low dimension this system is markedly stiff. The four dynamical variables H, Y, X, Z, and the constants A, B correspond to the concentrations of the chemical species H^+, HOBr, SO_3^{2-}, HSO_3^-, BrO_3^-, and $Fe(CN)_6^{4-}$, respectively. The two constants H_0 and X_0 are inflow concentrations of H^+ and SO_3^{2-} whereas the parameter k_0 describes the flow rate through the open system. The constants k_{-1} and $k_1,\ldots,k_5$ are kinetic rate constants associated with the set of chemical reactions on which the inorganic pH oscillator is based. Here we shall use the parameters k_0 and X_0 as bifurcation parameters. Numerical values used for the constants are summarized in Table V.

TABLE V. Rate constants and external constraints used for numerical simulations of the inorganic pH oscillator model in Eq. (23). All values are taken from Ref. 30.

Constant	Value
$k_1/M^{-1}s^{-1}$	5.0×10^{10}
k_{-1}/s^{-1}	3.0×10^{3}
$k_2/M^{-2}s^{-1}$	3.077×10^{6}
$k_3/M^{-1}s^{-1}$	10^{6}
k_4/s^{-1}	11.0
$k_5/M^{-1}s^{-1}$	2.5
A/M	6.5×10^{-2}
B/M	2.0×10^{-2}
H_0/M	2.0×10^{-2}

As illustrated in the bifurcation diagram in Fig. 4(a), the inorganic pH oscillator Eq. (23) exhibits oscillatory behavior emerging from Hopf bifurcation for a wide range of the parameters k_0 and X_0. Observe also that almost the entire curve in parameter space corresponds to subcritical Hopf bifurcations, except for a narrow region located at low flow

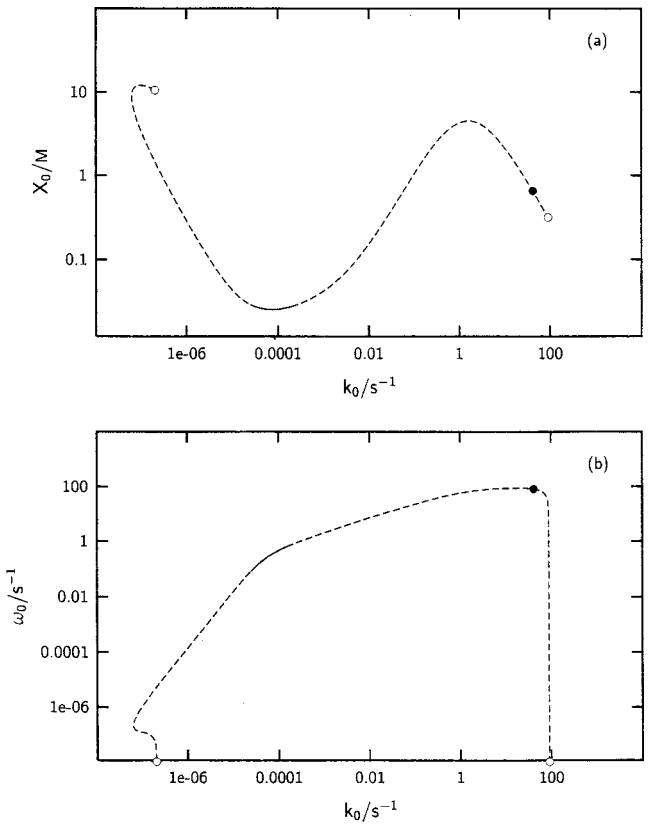

FIG. 4. Loci of Hopf bifurcations for the inorganic pH oscillator in the parameter plane (k_0, X_0). At two parameter points, the Hopf bifurcation changes stability from super- to subcritical (solid and dashed curves, respectively). The curve shown in (b) illustrates how the imaginary part ω_0 of the bifurcating eigenvalue varies along the bifurcation curve in (a).

TABLE VI. Characteristic coefficients for the normal form (10) associated with the Hopf bifurcation point in the inorganic pH oscillator (23) indicated on Fig. 4 with a solid circle.

	Re	Im
k_0	$4.111\,125\times10^{1}$	
X_0	$6.540\,699\times10^{-1}$	
ω_0	$7.993\,656\times10^{1}$	
λ_1	$1.013\,587\times10^{3}$	-5.406056×10^{2}
g	$-9.611\,112\times10^{8}$	2.052087×10^{9}

rates where the bifurcations are supercritical. Both endpoints on the bifurcation curve terminate at Bogdanov–Takens points indicated with white circles on Fig. 4. This feature is shown in Fig. 4(b) where the variation of the imaginary part ω_0 of the bifurcating eigenvalue along the bifurcation curve is shown as a function of the flow rate k_0; clearly, ω_0 vanishes at the two endpoints as required at a Bogdanov–Takens point.

To investigate the application of the higher-order expansions of Eq. (13) as the distance from the Hopf bifurcation point is varied, we have selected the sample point $(k_0, X_0) = (41.1112, 0.654\,069)$ marked on the bifurcation curve in Fig. 4 with a solid circle. The characteristics of the corresponding normal form are presented in Table VI.

Next, we keep X_0 fixed, and choose four increasing values of k_0 whose numerical values are shown in Table VII. Phase portraits showing the numerically accurate limit cycle solution and the first- and the third-order estimates of Eq. (13) projected onto the (H, X)-plane are shown in Fig. 5. For each of the four parameter values, the corresponding amplitudes of the oscillations for the two components H and X are shown in Table VII. Close to the bifurcation point (5a), both the first- and third-order estimate are numerically identical to the exact solution. However, as the distance is increased (5b) and (5c), deviations from the exact solution, become increasingly pronounced for the first-order estimate, whereas the third-order estimate still agrees well. Notice in Table VII that the size of the limit cycle increases by two orders of magnitude from cases (a)–(d). For a sufficiently large parameter value (5d) the third-order solution also fails to capture the dynamics and geometry of the exact solution.

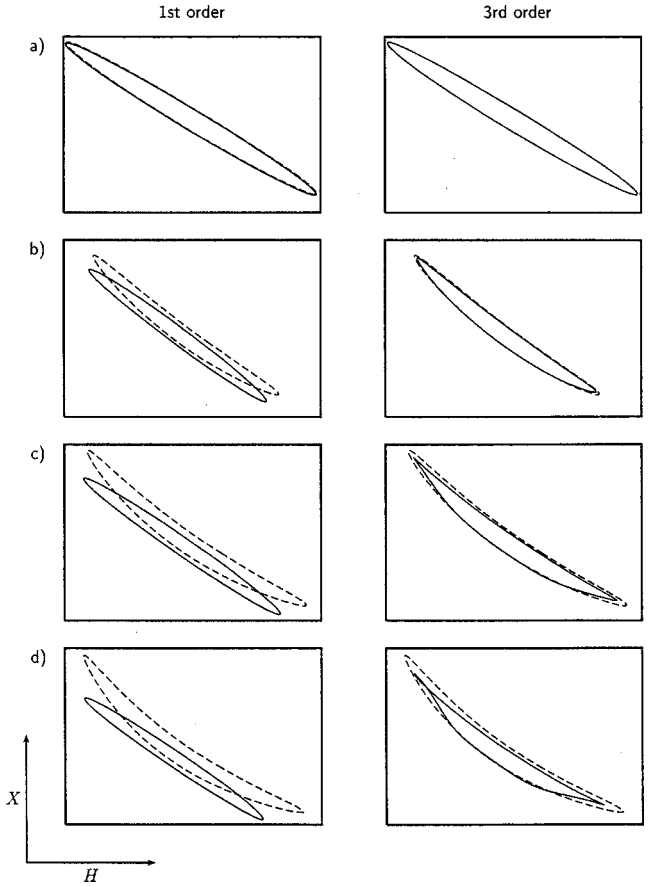

FIG. 5. Periodic solutions to the inorganic pH oscillator (23) (dashed lines) and approximations by the first- and third-order expansions of the limit cycle formula (13) (solid lines). The plots (a)–(d) represent projections of the closed orbit onto the (H,X)-plane and compare the limit cycle solutions at four increasingly larger values of the inflow parameter k_0 whose numerical values are shown in Table VII. The relative errors of the first- and third-order expansions compared to the exact limit cycle solutions are also displayed.

C. Peroxidase-oxidase oscillator

The purpose of the following example is to show the performance of the bifurcation formulas in Table I in a larger system whose dynamics are extremely stiff due to vastly different time scales involved. In addition, we illustrate the evolution of the periodic branches as they extend far from their emergence at the Hopf bifurcation. The system is a model for aerobic oxidation of nicotinamide adenine dinucleotide (NADH) catalyzed by the enzyme horseradish peroxidase. Apart from periodic oscillations emerging via a Hopf bifurcation the model exhibits a complex sequence of bifurcations leading to chaos. The model was proposed by Aguda and Larter[6] to account for earlier experimental observations of chaos.[31] The system is open to oxygen from air and is governed by ten evolution equations

$$
\begin{aligned}
\dot{A} &= -k_1WA + k_7CN,\\
\dot{B} &= k_2XN + k_3NY - k_4BZ - k_6BF + k_7CN - 2k_8B^2 \\
&\quad - k_{12}BW,\\
\dot{C} &= -k_5CW + k_6BF - k_7CN,\\
\dot{F} &= -k_6BF - k_{13}FV + k_t([\mathrm{O_2}]_{\mathrm{eq}} - F),\\
\dot{N} &= -k_2XN - k_3NY - k_7CN + \mathrm{NADH_{in}},\\
\dot{W} &= -k_1AW + k_3NY - k_5CW - k_{12}BW,\\
\dot{X} &= k_1AW - k_2XN + k_4BZ,\\
\dot{Y} &= k_2XN - k_3NY,\\
\dot{Z} &= -k_4BZ + k_5CW + k_{13}FV,\\
\dot{V} &= k_{12}BW - k_{13}FV,
\end{aligned}
\tag{24}
$$

where the variables are assigned to concentrations of respective species as follows: $A=[\mathrm{H_2O_2}]$, $B=[\mathrm{NAD}\cdot]$, $C=[\mathrm{O_2^-}]$,

TABLE VII. Four parameter values of inflow concentrations of hydrogen H_0 for the inorganic pH oscillator associated with the Hopf bifurcation point indicated on Fig. 4 with a solid circle. At each parameter value, the numerically accurate limit cycle solution and the first and third estimates provided by the expansion (13) have been calculated as shown in Fig. 5. The table also exhibits the amplitude of oscillations for both the H and X component at each corresponding parameter point.

Figure	$k_0-k_0^{\mathrm{Hopf}}$	Amplitude of H	Amplitude of X	$\lvert\mathbf{x}_1\rvert_{\mathrm{rel}}/\%$	$\lvert\mathbf{x}_3\rvert_{\mathrm{rel}}/\%$
5(a)	0.013 89	1.3652×10^{-6}	3.4583×10^{-9}	0.0230	0.0230
5(b)	0.013 96	2.1557×10^{-5}	5.5226×10^{-8}	3.6064	0.3628
5(c)	0.014 04	3.3952×10^{-5}	8.8395×10^{-8}	7.7942	1.3956
5(d)	0.014 13	4.6754×10^{-5}	1.2472×10^{-7}	13.2738	3.87005

$F=[O_2]$, $N=[\mathrm{NADH}]$, $W=[\mathrm{Per}^{3+}]$, $X=[\mathrm{coI}]$, $Y=[\mathrm{coII}]$, $Z=[\mathrm{coIII}]$, and $V=[\mathrm{Per}^{2+}]$. The various oxidation states of the enzyme are bound by the constraint $E_{\mathrm{tot}}=V+W+X+Y+Z$, which permits a reduction of the number of equations by one (we choose V to be calculated from the constraint and leave out the corresponding differential equation). The rate coefficients are fixed at $k_1,\ldots,k_4=k_6,\ldots,k_8=k_{12}=k_{13}=1\,\mu\mathrm{M}^{-1}\,\mathrm{s}^{-1}$, $k_5=60\,\mu\mathrm{M}^{-1}\,\mathrm{s}^{-1}$. Two external parameters, the mass transfer coefficient, $k_t=0.1\,\mathrm{s}^{-1}$, and the inflow of NADH, $\mathrm{NADH}_{\mathrm{in}}=0.1\,\mu\mathrm{Ms}^{-1}$, are also fixed. The remaining two parameters, the concentration of oxygen when equilibrated with the gas, $[O_2]_{\mathrm{eq}}$, and the total concentration of the enzyme, E_{tot}, are free.

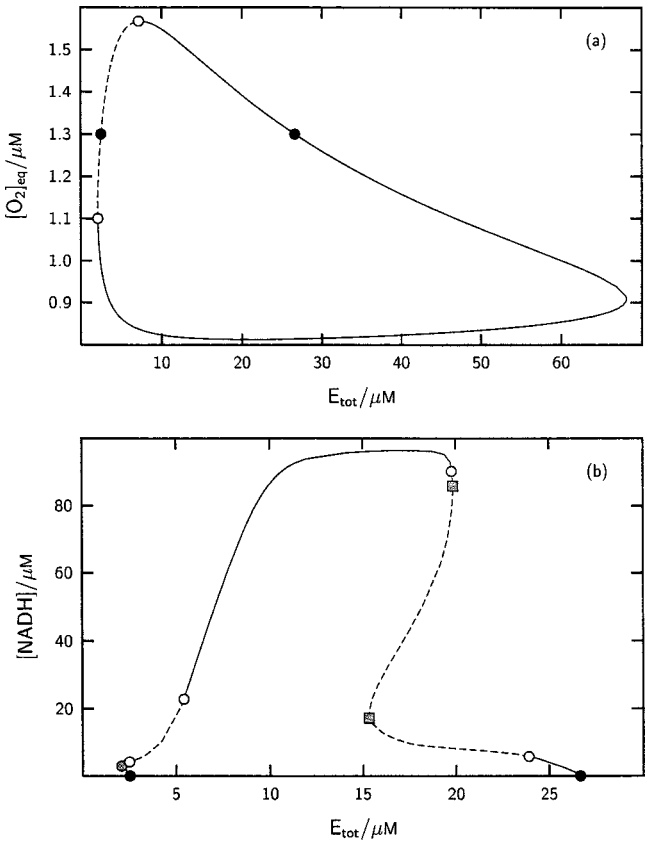

FIG. 6. (a) Loci of Hopf bifurcations for the peroxidase-oxidase oscillator in the parameter plane $([O_2]_{\mathrm{eq}},E_{\mathrm{tot}})$. Super- and subcritical regions are shown with solid and dashed curves, respectively. The curve shown in the solution diagram (b) illustrates a continuation of the limit cycles that branch off from the two Hopf bifurcation points marked in (a) with solid circles. Initial estimates of the limit cycle for a 20-point multiple shooting continuation were evaluated by using the full third expansion of Eq. (13). During the course of continuation the limit cycle exhibits a series of period-doubling and limit point bifurcations indicated on the continuation curve with white and gray circles, respectively.

The curve of the Hopf bifurcations in this parameter plane is shown in Fig. 6(a). It encloses a bounded region where oscillations are expected. Observe that the curve consists of both super- and subcritical parts as indicated by solid and dashed lines respectively.

The branches that emanate from the two bifurcation points selected by setting the parameter $[O_2]_{\mathrm{eq}}=1.3\,\mu\mathrm{M}$ are undergoing various bifurcations when further away from the Hopf bifurcation as shown in Fig. 6(b). The characteristics of the normal form are shown in Table VIII. The bifurcation formulas were used to find an estimate of a periodic orbit close to its emergence and this estimate was subsequently used to track the entire branch of periodic orbits by continuation. The figure shows that both Hopf points are joined by a single three times folded branch. The solutions become unstable due to repeated fold and period-doubling bifurcations, the latter being consistent with the observations of chaos discussed in Ref. 6.

D. Reaction-diffusion systems

As a final example, we wish to consider how the calculations of the characteristics of a Hopf bifurcation considered in the previous examples can be extended to reaction-diffusion systems described by a partial differential equation (PDE) of the form

TABLE VIII. Characteristic coefficients for the normal form (10) associated with the two Hopf bifurcation point in the peroxidase-oxidase model indicated on Fig. 6 with a solid circle.

	Re	Im
E_{tot}	$2.662\,883\times10^{1}$	
$[O_2]_{\mathrm{eq}}$	1.3	
ω_0	$1.052\,593\times10^{-2}$	
λ_1	$-2.777\,684\times10^{-5}$	$-2.151\,067\times10^{-5}$
g	$7.366\,951\times10^{-6}$	$1.848\,198\times10^{-5}$
E_{tot}	2.514 597	
$[O_2]_{\mathrm{eq}}$	1.3	
ω_0	$4.775\,365\times10^{-2}$	
λ_1	$8.274\,127\times10^{-4}$	$-1.228\,465\times10^{-3}$
g	$-8.655\,570\times10^{-5}$	$1.786\,902\times10^{-6}$

$$\frac{\partial \mathbf{x}}{\partial t} = \mathbf{J}\cdot\mathbf{x} + \mathbf{f}(\mathbf{x},\mu) + \mathbf{D}\cdot\nabla^2\mathbf{x}. \tag{25}$$

Here $\mathbf{x}(r,t)$ is a vector of n chemical components $x_i(r,t)$ defined on a functional space H dependent on both time t and a one-dimensional spatial variable r. The spatial dependence corresponds to the inclusion of diffusion driven transport of matter described by the diagonal diffusion matrix $\mathbf{D}$ whose individual components D_i are diffusion coefficients of the respective chemical species.

The extension and application of the center manifold theorem and bifurcation analysis in terms of normal form calculations for infinite dimensional systems of the type Eq. (25) is today well-established in the literature and we refer to Refs. 12, 15, 16 and 32 for a detailed treatment of this subject.

In this context, we wish to consider the Brusselator model[33] with an additional diffusion term, namely

$$\begin{aligned} \dot{x}_1 &= a-(b+1)x_1+x_1^2x_2+d\nabla^2 x_1, \\ \dot{x}_2 &= bx_1-x_1^2x_2+dq\nabla^2 x_2, \end{aligned} \tag{26}$$

where we shall use the diffusion coefficient d as the bifurcation parameter. The spatial variable r is defined on the domain $r\in[0;\pi]$ whereas each variable x_i is subject to no-flux (or von Neumann) boundary conditions

$$\left.\frac{\partial x_i}{\partial t}\right|_{r=0} = \left.\frac{\partial x_i}{\partial t}\right|_{r=\pi} = 0, \quad \text{for } i=1,2. \tag{27}$$

The Brusselator (26) has a nontrivial spatially homogeneous solution $(x_1^s,x_2^s)=(a,b/a)$ and we wish to consider the stability of this state here.

The linear part of Eq. (26) at the homogeneous state (x_1^s,x_2^s) defines an operator

$$\mathbf{M} = \mathbf{J} + \mathbf{D}\frac{\partial^2}{\partial r^2} \tag{28}$$

with eigenfunctions $\mathbf{\Upsilon}_k(r)$

$$\mathbf{\Upsilon}_k(r) = \cos(kr)\mathbf{v}_k, \tag{29}$$

where the wave number k is defined for $k=0,1,\ldots$. The vector $\mathbf{v}_k$ is the eigenvector associated with the eigenvalue problem

$$(\mathbf{J}-k^2\mathbf{D})\cdot\mathbf{v}_k = \lambda_k\mathbf{v}_k. \tag{30}$$

If we define an inner product $\langle\cdot,\cdot\rangle$ on the functional space H as

$$\langle \mathbf{w},\mathbf{v}\rangle = \sum_{i=1}^{2}\int_0^\pi \overline{w}_i v_i\, dr, \tag{31}$$

the adjoint operator $\mathbf{M}^*$ of Eq. (28) becomes

$$\mathbf{M}^* = \mathbf{J}^{\mathrm{T}} + \mathbf{D}\frac{\partial^2}{\partial s^2}, \tag{32}$$

with corresponding (adjoint) eigenfunctions

$$\mathbf{\Upsilon}_k^*(r) = \cos(kr)\mathbf{v}_k^*, \quad \text{for } k=1,2,\ldots. \tag{33}$$

As in Eq. (2), we normalize the eigenfunctions according to

$$\langle \mathbf{\Upsilon}_k^*, \mathbf{\Upsilon}_l\rangle = \delta_{kl}, \tag{34}$$

which implies that the right and left eigenvectors $\mathbf{v}_k$ and $\mathbf{v}_l^*$ satisfy

$$\mathbf{v}_k^*\cdot\mathbf{v}_l = \frac{2}{\pi}\delta_{kl}. \tag{35}$$

At the parameter value $d=2$, the homogeneous steady state undergoes a Hopf bifurcation for the wave number $k=1$, implying that a spatially nonhomogeneous periodic solution branches off from the homogeneous reference state $(a,b/a)$. The corresponding right and left eigenfunctions are

$$\mathbf{\Upsilon}(r) = \cos(r)\mathbf{v}, \quad \mathbf{\Upsilon}_1^*(r) = \cos(r)\mathbf{v}^*, \tag{36}$$

where

$$\mathbf{v} = (1,-2+\mathrm{i})^{\mathrm{T}}, \quad \mathbf{v}^* = \frac{1}{\pi}(1-2\mathrm{i},-\mathrm{i}). \tag{37}$$

By application of the inner product defined in Eq. (31), we may use the left eigenvector $\mathbf{\Upsilon}_1^*$ to decompose any smooth function in H into its center subspace component and associated complement.

For the example presented here, we only wish to discuss the calculation of the coefficients λ_1 and g of Eq. (10) and need therefore only to determine the coefficient vectors $\mathbf{h}_{200}$, $\mathbf{h}_{110}$, and $\mathbf{h}_{001}$. The notational modifications of the formulas in Table I needed to determine these quantities [and thereby the normal form equation (10) associated with the Hopf bifurcation] are almost trivial. For example, for the second-order component $\mathbf{h}_{200}(r)$, we find

$$(\mathbf{J}+\mathbf{D}\cdot\nabla^2-2\mathrm{i}\omega_0\mathbf{I})\cdot\mathbf{h}_{200} = -\tfrac{1}{2}\mathbf{F}_{\mathbf{xx}}(\mathbf{v},\mathbf{v}), \tag{38}$$

whereas the equation that determines the third-order coefficient g becomes

$$g = \langle \mathbf{v}^*, \mathbf{F}_{\mathbf{xx}}(\mathbf{v},\mathbf{h}_{110}) + \mathbf{F}_{\mathbf{xx}}(\overline{\mathbf{v}},\mathbf{h}_{200}) + \tfrac{1}{2}\mathbf{F}_{\mathbf{xxx}}(\mathbf{v},\mathbf{v},\overline{\mathbf{v}})\rangle. \tag{39}$$

Equation (38) is a linear boundary value problem which must be solved subject to the no-flux condition $\partial\mathbf{h}_{200}/\partial r = 0$. Insertion of $\mathbf{M}$ and the eigenfunction $\mathbf{\Upsilon}_1(r)$ into Eq. (38) gives

$$(\mathbf{J}+\mathbf{D}\cdot\nabla^2-2\mathrm{i}\omega_0\mathbf{I})\cdot\mathbf{h}_{200} = -(1+2\mathrm{i},-1-2\mathrm{i})^{\mathrm{T}}\cos^2 r. \tag{40}$$

Expanding the right-hand side as

$$(\mathbf{J}+\mathbf{D}\cdot\nabla^2-2\mathrm{i}\omega_0\mathbf{I})\cdot\mathbf{h}_{200} = \tfrac{1}{2}(1+2\mathrm{i},-1-2\mathrm{i})^{\mathrm{T}}(1+\cos 2r), \tag{41}$$

and solving Eq. (41) for each separate harmonic (1 and $\cos 2r$) gives

$$\begin{aligned} \mathbf{h}_{200}(r) = (1+2\mathrm{i})[&-\tfrac{1}{15}(2+\mathrm{i},\tfrac{15}{6})^{\mathrm{T}} \\ &+-\tfrac{1}{51}(4-\mathrm{i},-\tfrac{255}{31}+4\mathrm{i})^{\mathrm{T}}\cos 2r]. \end{aligned} \tag{42}$$

The derivations and solutions of the linear equations that determine the remaining quantities from Table I (the transformation coefficients $\mathbf{h}_{110},\mathbf{h}_{210},\mathbf{h}_{300}$, as well as the unfolding coefficient λ_1) follow precisely the same procedure sketched for $\mathbf{h}_{200}$ above and we shall therefore omit these details here. Using the same procedure as demonstrated for $\mathbf{h}_{200}$, we find for the additional coefficient functions

TABLE IX. Numerically calculated values of the nonlinear coefficient g of the normal form Eq. (10) for the Brusselator PDE (26) using second- and fourth-order finite difference schemes for discretization of the Laplacian. For an increasing number of grid points, each row displays the numerically obtained values as well as the relative error with respect to the exact solution shown in Eq. (44).

	Normal form coefficient g			
Grid points	2. order	4. order	Relative error/%	
16	$3.432\,284\,5 - i3.090\,980\,7$	$3.435\,875\,1 - i3.091\,076\,3$	0.080	0.002
32	$3.435\,121\,9 - i3.091\,061\,1$	$3.435\,974\,5 - i3.091\,078\,3$	0.019	1.2×10^{-4}
64	$3.435\,772\,9 - i3.091\,074\,2$	$3.435\,980\,0 - i3.091\,078\,4$	0.005	7.4×10^{-6}
128	$3.435\,929\,3 - i3.091\,077\,4$	$3.435\,980\,3 - i3.091\,078\,4$	0.001	4.6×10^{-7}

$$\mathbf{h}_{110}(r) = \tfrac{1}{25}(4\cos 2r, -25 - 9\cos 2r)^{\mathrm{T}},$$
$$\mathbf{h}_{001}(r) = 0. \tag{43}$$

Using the definition of the inner product (31), the third-order coefficient g is calculated from Eq. (39) as

$$g = -\frac{35\,047}{10\,200} + \mathrm{i}\frac{31\,529}{10\,200}, \tag{44}$$

whereas a similar calculation for λ_1 gives

$$\lambda_1 = -\tfrac{3}{4} + \mathrm{i}\tfrac{1}{2}. \tag{45}$$

A similar calculation for the Brusselator PDE system Eq. (26) has also been discussed in Ref. 34 using, however, different settings for the boundaries of the physical domain.

To test the accuracy of the numerical code that was used in the previous three examples for location of the Hopf bifurcation and evaluation of the terms in the limit cycle expansion (13), we have compared the numerical calculations of the nonlinear coefficient g with the analytic values Eqs. (44) and (45). To transform the Brusselator PDE (26) into a set of ODE's, we have used a standard second- and fourth-order finite difference scheme for discretizing the Laplacian operator. Note that no special care was taken to make use of the special sparse banded structure of the Jacobian matrix which occur in this context.

The results are exhibited in Table IX where the numerical values of g and the corresponding relative error of the absolute value are shown for an increasing number of grid points for the two finite difference schemes. As expected, the error decreases with the number of grid points used in both the second- and fourth-order approximations. However, the numbers also clearly show that the fourth-order approximation is highly superior compared to the second-order discretization: Even for relatively small spatial resolutions (32 grid points), the fourth approximation is correct within $1.2\times10^{-4}\%$ of the analytic value. A similar conclusion for the Brusselator model regarding the accuracy of finite difference schemes was pointed out in a somewhat different context in a paper by Wittenberg and Holmes.[35]

V. DISCUSSION

The numerical analysis of Hopf bifurcation points should meet at least two criteria: First, the method should provide a sufficiently precise initial estimate for a one-parameter continuation of the periodic orbit which emerges at the Hopf bifurcation point. Second, the method should provide information regarding the stability of the limit cycle close to the bifurcation point by determining whether the Hopf bifurcation is super- or subcritical.

In this paper, we have shown how these two criteria can be met efficiently by a straightforward application of the normal form theorem. We provide explicit expressions for deriving the nonlinear contributions from the normal form transformation for the expansion of the limit cycle emerging at a Hopf bifurcation. All the examples considered here clearly illustrate that the addition of the nonlinear terms to the limit cycle expansion provides a significant improvement and accuracy in the numerical estimate of the limit cycle. This can be crucial for the convergence. We stress that the calculation of the additional nonlinear terms requires very little extra numerical work since these terms are required for the determination of the resonant coefficients in the corresponding normal form (10) for the Hopf bifurcation. In fact, only the third-order terms in the expansion requires additional numerical work. We believe these results will prove useful for future developments of robust numerical codes for bifurcation analysis of Hopf bifurcations superseding currently used ones.

In addition, we have also shown that inclusion of higher-order terms in the normal form approximation provides a significant improvement in the representation of the exact limit cycle. This, for example, is clearly illustrated in Fig. 5, where both the translation and the nonlinear bending of the limit cycle is captured well by the higher-order expansion. This holds even at parameter distances quite far from the actual Hopf bifurcation point and makes it much easier for the numerical procedure of finding the limit cycle to converge. In addition, we believe that this may have experimental importance when the geometry of the limit cycle is reconstructed from experimental data using either quenching techniques[36] or control theory.[37]

The ideas presented here for the Hopf bifurcation have been implemented numerically into a software tool BRANCH[38] which supports bifurcation analysis of dynamical systems described by autonomous ordinary differential equations and discrete iterated maps. For such systems, all ''simple'' codimension-one bifurcations are handled: Saddle-node, transcritical, pitchfork, and Hopf–Neimark-Sacker bifurcations of stationary, periodic, and fixed point solutions, as well as period doubling bifurcations of periodic orbits. In addition, a range of codimension-two bifurcations commonly encountered in ODE's with special symmetry

properties are also supported. For the analysis of periodic solutions of Eq. (1), full support for multiple shooting or discretization is provided. Estimates of initial points on the branches are calculated and output is generated in a form suitable as input data for the continuation software CONT [Ref. 18 (Appendix B)]. Both software packages are free and can be obtained by contacting the authors.

Finally, we emphasize that the results presented in this paper have general relevance within the field of dynamical systems and nonlinear dynamics: Even though the examples and the discussion are focused on nonlinear chemical kinetics, the Hopf bifurcation formulas in Table I can be applied to any dynamical system represented by a set of autonomous ordinary differential equations of the form (1).

[1] B. P. Belousov, *Sbornik referatov po Radiatsionnoi Meditsine* (Medgiz, Moscow, 1959), p. 145, collections of abstracts on radiation medicine (in Russian).
[2] A. M. Zhabotinsky, Biophysics (Engl. Transl.) **9**, 306 (1964).
[3] A. N. Zaikin and A. M. Zhabotinsky, Nature (London) **255**, 535 (1970).
[4] R. J. Field and M. Burger, *Oscillation and Travelling Waves in Chemical Systems* (Wiley-Interscience, New York, 1985).
[5] A. M. Zhabotinsky, Chaos **1**, 379 (1991).
[6] B. D. Aguda and R. Larter, J. Am. Chem. Soc. **113**, 7913 (1991).
[7] R. Larter, L. F. Olsen, C. G. Steinmetz, and T. Geist, in *Chaos in Chemistry and Bicohemistry*, edited by R. J. Field and L. Györgyi (World Scientific, Singapore, 1993), pp. 175–224.
[8] C. G. Hocker *et al.*, Biophys. Chem. **51**, 21 (1994).
[9] I. Schreiber, P. Hasal, and M. Marek, Chaos **9**, 43 (1999).
[10] E. Hopf, Ber. Math.-Phys. Kl. Sächs Acad. Wiss. Leipzig **94**, 1 (1942) (a translation of this paper, and comments on it appear as Section 5 of Ref. 11).
[11] J. E. Marsden and M. McCracken, *The Hopf Bifurcation and Its Applications* (Springer-Verlag, New York, 1976).
[12] B. D. Hassard, N. D. Kazarinoff, and Y.-H. Wan, *Theory and Applications of Hopf Bifurcation, No. 41 in London Mathematical Society Lecture Note Series* (Cambridge University Press, Cambridge, 1981).
[13] Y. Kuramoto, *Chemical Oscillations, Waves, and Turbulence* (Springer-Verlag, Berlin, 1984).
[14] J. Guckenheimer and P. J. Holmes, *Nonlinear Oscillations, Dynamical Systems and Bifurcations of Vector Fields* (Springer-Verlag, New York, 1983).
[15] J. Carr, *Applications of Center Manifold Theory* (Springer-Verlag, New York, 1981).
[16] Y. A. Kuznetsov, *Elements of Applied Bifurcation Theory* (Springer-Verlag, New York, 1995).
[17] M. Kubíček and M. Marek, *Computational Methods in Bifurcation Theory and Dissipative Structures* (Springer-Verlag, New York, 1983).
[18] M. Marek and I. Schreiber, *Chaotic Behavior of Deterministic Dissipative Systems* (Cambridge University Press, Cambridge, 1995).
[19] M. Ipsen, F. Hynne, and P. G. Sørensen, Chaos **8**, 834 (1998).
[20] T. Kato, *Perturbation Theory for Linear Operators* (Springer-Verlag, Berlin, 1966).
[21] W.-J. Beyn, in *Nonlinear Partial Differential Equations and Dynamical Systems*, Vol. 1 of *Advances in Numerical Analysis*, edited by W. Light (Clarendon, Oxford, 1991), Chap. 5, pp. 175–236.
[22] M. Holodniok and M. Kubíček, Appl. Math. Comput. **15**, 261 (1984).
[23] *Handbook of Mathematical Functions*, edited by M. Abramowitz and I. A. Stegun (Dover, New York, 1964).
[24] E. Doedel, H. B. Keller, and J. P. Kernevez, Int. J. Bifurcation Chaos Appl. Sci. Eng. **1**, 493 (1991).
[25] E. Anderson *et al.*, LAPACK *Users's Guide*, 2nd ed. (SIAM, Philadelphia, 1995).
[26] A. C. Hindmarsh, in *Scientific Computing*, edited by R. S. Stepleman *et al.* (North-Holland, Amsterdam, 1983), pp. 55–64.
[27] S. R. Caplan, A. Naparstek, and N. J. Zabusky, Nature (London) **245**, 364 (1973).
[28] A. Naparstek, S. R. Caplan, and D. Thomas, Biochim. Biophys. Acta **323**, 643 (1973).
[29] F. Takens, Institut des Hautes Études Scientifiques **43**, 47 (1974).
[30] Y. Luo and I. R. Epstein, J. Am. Chem. Soc. **113**, 1518 (1991).
[31] L. F. Olsen and H. Degn, Nature (London) **267**, 177 (1977).
[32] G. Iooss and D. D. Joseph, *Elementary Stability and Bifurcation Theory*, 2nd ed. (Springer-Verlag, New York, 1980, 1990).
[33] R. Lefever and I. Prigogine, J. Chem. Phys. **48**, 263 (1968).
[34] Y. Kuramoto and T. Tsuzuki, Prog. Theor. Phys. **54**, 687 (1975).
[35] R. Wittenberg and P. Holmes, Physica D **100**, 1 (1997).
[36] F. Hynne, P. G. Sørensen, and K. Nielsen, J. Chem. Phys. **92**, 1747 (1990).
[37] E. Mihaliuk, H. Skødt, F. Hynne, P. G. Sørensen, and K. Showalter, J. Phys. Chem. A **103**, 8246 (1999).
[38] M. Ipsen, Technical report, UNI-C (unpublished).